

Online Learning Based Mobile Robot Controller Adaptation for Slip Reduction

Huidong Gao* Rui Zhou* Masayoshi Tomizuka* Zhuo Xu*

* Department of Mechanical Engineering, University of California, Berkeley, CA 94720 USA (e-mail: {hgao9, ruizhouzr, tomizuka, zhuoxu}@berkeley.edu)

Abstract:

Slip is a very common phenomena present in wheeled mobile robotic systems. It has undesirable consequences such as wasting energy and impeding system stability. To tackle the challenge of mobile robot trajectory tracking under slippery conditions, we propose a hierarchical framework that learns and adapts gains of the tracking controllers simultaneously online. Concretely, a reinforcement learning (RL) module is used to auto-tune parameters in a lateral predictive controller and a longitudinal speed PID controller. Experiments show the necessity of simultaneous gain tuning, and have demonstrated that our online framework outperforms the best baseline controller using fixed gains. By utilizing online gain adaptation, our framework achieves robust tracking performance by rejecting slip and reducing tracking errors when the mobile robot travels through various terrains.

Keywords: Trajectory Tracking, Slip Rejection, Reinforcement Learning, Hierarchical Control

1. INTRODUCTION

1.1 Background and Motivation

Mobile robots are used in various industrial applications such as manufacturing, process and aerospace. They often run on slippery terrains, or routes with rapid cornering, which induces skidding and slipping. Excessive slip may cause motion instability, undermine maneuverability and lead to possible collisions, thus should be prevented.

To mitigate slip, many works try to identify slip parameters or terrain states, and design simple control laws with robot kinematic models, e.g. Pico et al. [2022] and Kim and Lee [2016]. Sebastian and Ben-Tzvi [2019] and Wang and Zhai [2020] further choose to model slip as disturbance in the kinematics model and estimate by observers. However, state vectors are of high order and matrix inverse calculations could be massive. Another line of work focuses on wheel dynamics with traction forces. Tian et al. [2009] choose to use the Magic formula to derive the relationship between traction force and slip ratio, while Nandy et al. [2011] formulates a detailed slip dynamics with certain switching conditions. Although dynamic models consider forces in addition to kinematics models, they usually require system identification for different scenarios and have poor generalization abilities.

There are also other works utilizing reinforcement learning to directly learn a policy; such as in Xu et al. [2018], Tang et al. [2019], Chang et al. [2020], Cai et al. [2020], Xu et al. [2021]. However, end-to-end RL approaches require considerable training time and pose challenges in explainability. Instead of end-to-end RL, Carlucho et al. [2019], Gao et al. [2022] uses RL only to optimize controllers, but the results are highly dependent on action space discretization.

1.2 Contributions

Our work focuses on trajectory tracking control of mobile robots under slippery conditions. We follow a similar approach as in Carlucho et al. [2019], and propose to use a hierarchical framework that optimizes gains for the tracking controllers online. An RL module is used to tune gains in a lateral predictive Stanley controller and a longitudinal speed PID controller simultaneously for regulation. By dividing the control part into longitudinal and lateral control modules and tuning gains directly, we are able to improve lateral and speed tracking errors in a straightforward way. By using a higher level RL module, we are able to tune multiple low-level controllers simultaneously in real-time. Furthermore, the RL module is only able to determine the conservativeness in the controllers, and thus the entire framework is more explainable than an end-to-end RL controller.

The contributions of our work can be summarized as follows: 1) We propose an hierarchical framework that actively optimizes controllers to slip conditions through RL gain-tuning. 2) We reason the necessity of simultaneous online gain tuning through experiments. 3) We demonstrate that our adaptive framework outperforms the best fixed-gain baselines by 6.6% and 12.7% for average lateral error and max lateral error by simulation.

2. METHODOLOGY

2.1 Problem Overview

Fig. 1 illustrates our tracking problem layout. The robot's goal is to travel from x_{start} , following a predefined trajectory to reach x_{end} . Here we define certain terms to describe the robot's motion and the tracking state. We use lateral

displacement error e to represent the closest tracking error relative to the reference trajectory (in unit m). $\Delta\theta$ is the yaw error, which is the difference between reference yaw θ_{ref} and actual yaw θ (in unit rad). Δv is the speed error, which is the difference between absolute values of reference velocity v_{ref} and actual velocity v (in unit m/s).

The tracking task can then be formulated as a Markov Decision Process defined by $\mathcal{M} = (\mathcal{S}, \mathcal{A}, \mathcal{T}, \mathcal{R}, \gamma)$. \mathcal{S} represents the state space; \mathcal{A} is the action space; $\mathcal{T}(s|s, a)$ is the state transition model; $\mathcal{R}(s, a)$ is the reward function; and $\gamma \in [0, 1)$ is the discount factor. The RL formulation aims to learn a policy $\pi(a|S)$. The agent then follows the policy π , obtains an observation s_t at time t and performs an action a_t . It then receives from the environment a reward R_t and a new observation s_{t+1} , and π is updated accordingly. The final trained model gives an action selection policy π that maximizes the expectation of a discounted sum of rewards $E[\sum_{t=1}^T \gamma^{t-1} R_t]$.

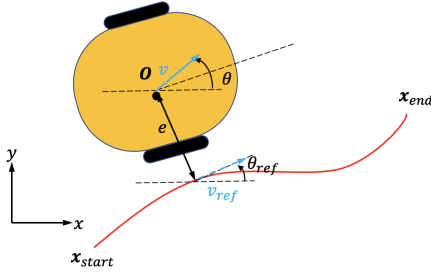


Fig. 1. Schematic diagram of the problem setup.

The state S has 5 variables: e , $\Delta\theta$, Δv , $\Delta v_{c-vs-actual}$, and $\Delta\omega_{c-vs-actual}$. e , $\Delta\theta$, and Δv are as discussed in the beginning of the section. $\Delta v_{c-vs-actual}$ (in unit m/s) and $\Delta\omega_{c-vs-actual}$ (in unit rad/s) represent the difference between actual body velocities and body velocities calculated from wheel velocity commands (shown in Eqn. 1 and 2). Intuitively, a large value of $\Delta v_{c-vs-actual}$ or $\Delta\omega_{c-vs-actual}$ indicates the robot is slipping more severely as the wheel velocity commands are not fully transferred to actual body velocities.

$$v = \frac{(\omega_R + \omega_L) \cdot R}{2} \quad (1)$$

$$\omega = \frac{(\omega_R - \omega_L) \cdot R}{b} \quad (2)$$

Eqn. 1-2: transformation from wheel commands to calculated body linear and angular velocities. ω_R and ω_L are right and left wheel angular velocity commands, R is wheel radius, and b is distance between wheels.

The action A is $[v, \omega]$, which are linear and angular velocity commands. Notice the final input wheel velocity commands are calculated from reversing equations 1-2. The low level controller executes the commands and gets a reward at this step. The reward for each step is defined in Eqn. 3. Here we penalize e , $\Delta\theta$ and Δv , with coefficients R_{dist} , R_{ang} and R_{speed} . The cumulative reward is defined as $\sum_{t=1}^T \gamma^{t-1} R_t$, where R_t is the step reward.

$$R_t(s_t, a_t) = R_{dist} \cdot e^2 + R_{ang} \cdot \Delta\theta^2 + R_{speed} \cdot \Delta v^2 \quad (3)$$

2.2 Proposed Framework

We propose to utilize reinforcement learning to actively tune parameters in lateral and longitudinal control modules on a differential drive TurtleBot. The proposed framework consists of a RL-based high-level module, a lateral control module, a longitudinal control module, a low-level tracking controller, and the robot. The framework is visualized in Fig. 2. The RL module takes observed robot states obs ; reference trajectory x_{ref} , and outputs gains $K_{stanley}$ and K_{speed} . The two control modules use the gains accordingly and output acceleration command α and steering angle command δ , and then transfer them into linear and angular velocity commands $[v, \omega]$. The low level controller then executes the command on the robot and feeds the directly observed states back into the RL module to calculate for step rewards, and the policy is updated accordingly. The loop stops when the positional error of the robot and final goal position is within a threshold. The entire framework realizes our MDP formulation, and is trained end-to-end using an RL algorithm.

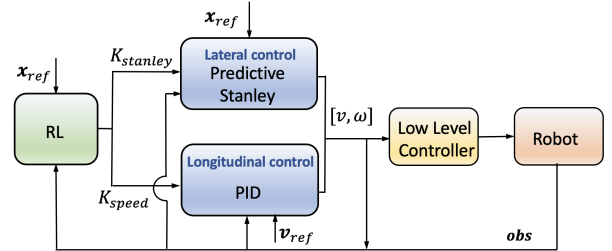


Fig. 2. Proposed framework.

2.3 Lateral Control: Predictive Stanley

We tackle our trajectory tracking problem by breaking it up into longitudinal and lateral control problems. The longitudinal controller is responsible for regulating the robot's speed while the lateral controller aims to reduce the lateral error during path tracking.

The proposed lateral control approach utilizes a version of Predictive Stanley controller, which is built on the basic Stanley controller. The basic Stanley controller is divided into three regions: saturated low region, saturated high region, and nominal region. ψ is the heading of the vehicle with respect to the heading of the trajectory at the point of the projected shortest distance to the vehicle position, $e(t)$ is the lateral error, v is current speed, and $K = K_{stanley}$ is the controller gain. See Fig. 3 for reference. The steering angle command is given by:

$$\delta(t) = \begin{cases} \psi(t) + \arctan\left(\frac{Ke(t)}{v(t)}\right), & |\psi(t) + \arctan\left(\frac{Ke(t)}{v(t)}\right)| < \delta(max) \\ \delta(max), & \psi(t) + \arctan\left(\frac{Ke(t)}{v(t)}\right) > \delta(max) \\ -\delta(max), & \psi(t) + \arctan\left(\frac{Ke(t)}{v(t)}\right) < -\delta(max) \end{cases} \quad (4)$$

As discussed in AbdElmoniem et al. [2020], the proposed predictive Stanley control approach introduces a third input, which is a developed array of future vehicle states, propagated along the vehicle track, denoted as $P_1, P_2 \dots P_N$

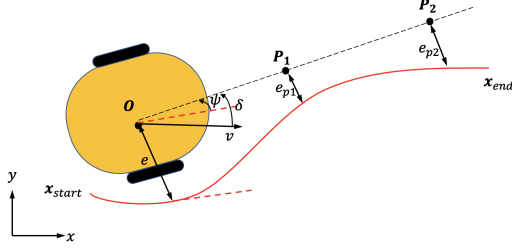


Fig. 3. Predictive Stanley Representation.

as shown in Fig. 3. At each future state, the corresponding δ is calculated based on current e_{pi} . The final steering angle command is calculated by augmenting the output of each basic Stanley controller at each state to eliminate the error along the path not only at the reference point, as shown in Eqn. 5 and 6. Consequently, the predictive Stanley controller is able to deal with the sudden changes in the heading angle of the trajectory by having this preview capability.

$$\delta(t) = \sum_{i=0}^N p_i [\psi_i(t) + \arctan(\frac{K e_{pi}(t)}{v(t)})] \quad (5)$$

$$p_i = p_{i-1}^2 \text{ for } i = 2 \dots N \quad (6)$$

Eqn. 5-6. The final steering command. p_i is the weight, which represents how each controller contributes in determining the final value of the steering angle. Here we set $N = 2$ and $p_1 = 0.2$.

We show the advantage of our predictive Stanley controller over the basic Stanley controller by running them on a TurtleBot with the same trajectory. The visualization in Fig. 4 clearly shows that the predictive Stanley controller is able to adjust for abrupt turns. See detailed comparison in AbdElmoniem et al. [2020].

2.4 Longitudinal Control: PID

We use a simple proportional control for speed regulation. The acceleration command becomes:

$$\alpha(t) = K_{speed}(v_{ref} - v(t)) \quad (7)$$

With the steering and acceleration commands, we can deduce the robot's linear and angular velocity commands $[v, \omega]$ using Eqn. 8 and 9, which are then executed by the low level controller.

$$v_{command} = v(t) + \alpha(t) \cdot \Delta T \quad (8)$$

$$\omega_{command} = \frac{\delta(t)}{\Delta T} \quad (9)$$

2.5 Reinforcement Learning module

The RL module in Fig. 2 consists of actor and critic neural network layers. The entire framework in Fig. 2 utilizes soft actor-critic (SAC) during training.

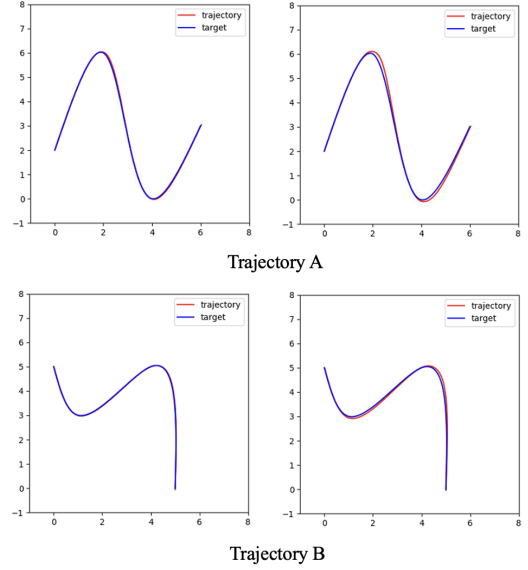


Fig. 4. Predictive Stanley vs. Basic Stanley Controller. The average lateral error for trajectory A for predictive and basic Stanley controllers are $0.0147m$ and $0.0374m$, respectively; for trajectory B are $0.0077m$ and $0.0347m$, respectively.

3. EXPERIMENTS

Our experiments were designed and conducted in order to answer the following questions:

- (1) Is simultaneous gain tuning necessary?
- (2) Is online gain tuning better than fixing the gains throughout the trajectory?
- (3) How to interpret our framework's output?

To answer these questions, we carry out simulated experiments using PyBullet by Coumans and Bai [2016–2021], with a TurtleBot waffle-pi model. To evaluate our framework, we propose to use a set of long-term and short-term metrics. Long-term metrics focus on measuring the performance throughout the entire trajectory, while short-term metrics focus on the short-time performance while the robot is slipping. Here we define slipping condition as those robot body states satisfying $\Delta v_{c-vs_actual} > |0.7| m/s$ or $\Delta \omega_{c-vs_actual} > |3| rad/s$.

For long-term criteria, we define average episodic reward \bar{r} , average lateral error \bar{e} , average speed error $\bar{\Delta v}$, and average RMS of change in low level control command $\bar{\Delta \mathbf{u}}$ (which measures command stability). $\mathbf{u} = [\omega_L, \omega_R]$, which denotes left and right wheel velocity control action commands, and is calculated based on $[v, \omega]$, using Eqn. 1 and 2. The long-term metrics are calculated with respect to the entire trajectory.

$$\bar{r} = \frac{1}{T_{traj}} \sum_{i=0}^{T_{traj}} r_i \quad (10)$$

$$\bar{e} = \frac{1}{T_{traj}} \sum_{i=0}^{T_{traj}} e_i \quad (11)$$

$$\overline{\Delta v} = \frac{1}{T_{traj}} \sum_{i=0}^{T_{traj}} |v_i - v_{ref}|, \quad (12)$$

$$\overline{\Delta \mathbf{u}} = \frac{1}{T_{traj}} \sum_{i=1}^{T_{traj}} \|\mathbf{u}_{i+1} - \mathbf{u}_i\|, \quad (13)$$

For short-term criteria, we define max lateral error throughout the trajectory e_{max} , average lateral error during slipping $(T_{slip}) \bar{e}_{slip}$, average speed error during slipping $\overline{\Delta v}_{slip}$, and average RMS of change in low level control action during slipping $\overline{\Delta \mathbf{u}}_{slip}$.

$$e_{max} = \max\{e_i\}_{i=0}^{T_{traj}} \quad (14)$$

$$\bar{e}_{slip} = \frac{1}{T_{slip}} \sum_{i=0}^{T_{slip}} e_i \quad (15)$$

$$\overline{\Delta v}_{slip} = \frac{1}{T_{slip}} \sum_{i=0}^{T_{slip}} |v_i - v_{ref}|, \quad (16)$$

$$\overline{\Delta \mathbf{u}}_{slip} = \frac{1}{T_{slip}} \sum_{i=1}^{T_{slip}} \|\mathbf{u}_{i+1} - \mathbf{u}_i\|, \quad (17)$$

3.1 Simulation environment setup and training

Fig. 5 shows bird-eye view simulation renderings of three example setups. Blue color represents high frictional areas with frictional coefficient $\mu=0.9$, and red represents low frictional areas with $\mu=0.01$. The red patches are of size 1 m by 1 m. The green trajectory is generated using a spline generator by Sakai et al. [2018]. The planner takes n number of 2D points and generates a smooth trajectory connecting all the given points.

To randomize the trajectory, we choose to use 5 random points for curve generation. Each point is *Uniform*[1, 2] m away from the previous point, with *Uniform*[-0.5 π , 0.5 π] rad angle from the previous point. The initial point $[x, y]$ position follows distribution: $x = \text{Uniform}[1, 2]$ m, $y = \text{Uniform}[3.5, 4.5]$ m.

To randomize the ground configuration, the red patches are randomly generated for each new trajectory, and we set 30% of the total area to be red.

We use SAC algorithm to train the entire framework. The policy network and the value network in the SAC are fully-connected two-layer neural networks of size 64. Learning rate is 0.0006, γ is set to be 0.99. The coefficients R_{dist} , R_{ang} and R_{speed} are set to be -20, -1, -1, respectively. The entire framework is trained until convergence.

3.2 Is simultaneous gain tuning necessary?

We propose to utilize RL to tune the two gains simultaneously, rather than having two separate frameworks to determine each. To verify the necessity of simultaneous gain tuning, we vary $K_{stanley}$ and K_{speed} from 0.5 to 5.0 with 0.5 increments, and plot heatmaps for each of the

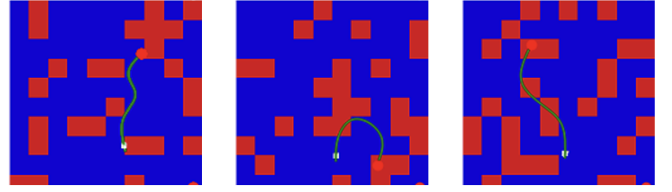


Fig. 5. **Simulation Rendering.** Bird-eye view image with annotations. White dot is the robot, green line is the reference trajectory, and red dot is the goal position.

criteria discussed previously (Fig. 6 and 7). Each point on the heatmap represents the result of using a specific combination of $K_{stanley}$ and K_{speed} . Each point result is calculated by averaging the results of running 100 pre-generated random trajectories with random ground setups.

It can be shown that for each criteria, the best result happens when considering $K_{stanley}$ and K_{speed} together. For example, for \bar{e} , fixing $K_{stanley}$ to be 2.5 will result in a best K_{speed} of 3.5, but fixing $K_{stanley}$ to be 5.0 will result in a best K_{speed} of 2.0. Therefore the gains have to be tuned simultaneously in order to achieve the best results.

For different criteria, the optimum happens at different combinations of $K_{stanley}$ and K_{speed} , because the criteria are focused on different aspects. For instance, to stabilize command and reduce $\overline{\Delta \mathbf{u}}$, \bar{e} may be compromised because commands need to be tuned less abruptly.

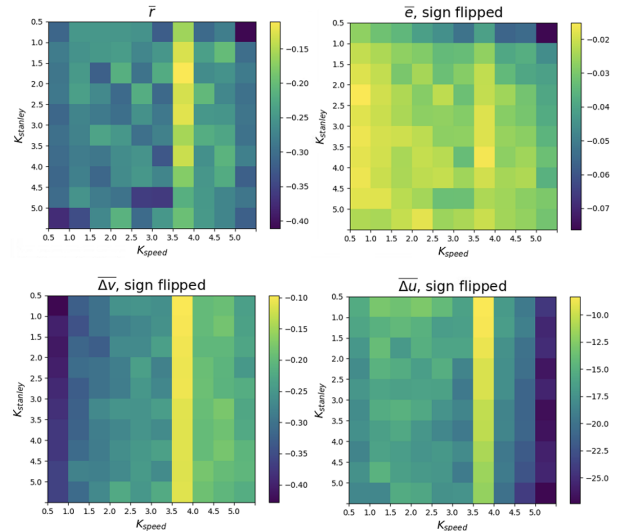


Fig. 6. **Parameter sweeping results for long-term metrics**

3.3 Is online gain tuning better than fixed parameters?

We propose to tune the gains online throughout the entire trajectory rather than using fixed gains. To verify this, we use a baseline model. The baseline model uses the same framework as in Fig. 2, but without the RL module. Instead of varying the two gains online, the baseline model utilizes fixed best gains found by offline parameter sweeping in $K_{stanley}$ and K_{speed} . The best gain combinations of baseline model for each metric is shown in the second column in *Parameter Sweeping* in Tables 1 and 2. We run the same 100 pre-generated random

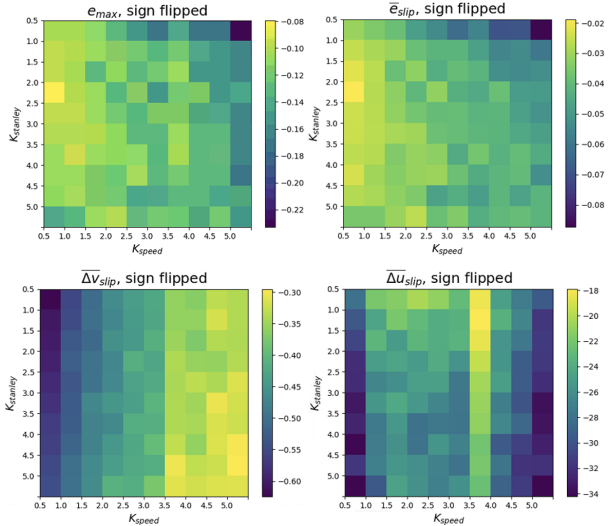


Fig. 7. Parameter sweeping results for short-term metrics

trajectories for the baseline model and our trained model, and log the results in the two tables. It can be shown that our framework is able to improve \bar{e} , e_{max} , \bar{e}_{slip} by 6.6%, 12.7%, and 4.7%, respectively.

One thing to notice is that the best results for each metric happens at different gain combinations with the baseline parameter-sweeping model. For example \bar{e} has best results when setting $K_{stanley} = 2.0$ and $K_{speed} = 0.5$, but for $\bar{\Delta u}$ it's $K_{stanley} = 0.5$ and $K_{speed} = 3.5$, which means the baseline model will perform worse if using the same combination of gains for all metrics. However our model is still able to beat the best of each baseline model metric with a universal trained policy, in lateral error metrics and $\bar{\Delta u}$ metric.

Table 1. Long-term metrics comparison.

The second column in Parameter Sweeping indicates at what value of gains the best metric result was obtained.

Metrics	Parameter Sweeping	Proposed Framework	Improvement
$(-)\bar{r}$	0.110 ± 0.118 $K_{stanley} = 1.5$ $K_{speed} = 3.5$	0.084 ± 0.125	23.6%
\bar{e}	0.015 ± 0.010 $K_{stanley} = 2.0$ $K_{speed} = 0.5$	0.014 ± 0.017	6.6%
$\bar{\Delta v}$	0.096 ± 0.042 $K_{stanley} = 0.5$ $K_{speed} = 3.5$	0.097 ± 0.058	-1.0%
$\bar{\Delta u}$	8.320 ± 2.040 $K_{stanley} = 0.5$ $K_{speed} = 3.5$	5.917 ± 2.165	28.9%

Table 2. Short-term metrics comparison.

Metrics	Parameter Sweeping	Proposed Framework	Improvement
e_{max}	0.079 ± 0.055 $K_{stanley} = 2.0$ $K_{speed} = 0.5$	0.069 ± 0.066	12.7%
\bar{e}_{slip}	0.021 ± 0.013 $K_{stanley} = 2.0$ $K_{speed} = 0.5$	0.020 ± 0.032	4.7%
$\bar{\Delta v}_{slip}$	0.295 ± 0.082 $K_{stanley} = 4.5$ $K_{speed} = 5.0$	0.42 ± 0.087	-42.3%
$\bar{\Delta u}_{slip}$	18.9 ± 5.93 $K_{stanley} = 1.0$ $K_{speed} = 3.5$	21.27 ± 4.76	-12.5%

3.4 Explainability of our framework output

We visualize two setup results in Fig. 8 and 9. The upper figures show the baseline model with best gain combinations, and the lower figures show our model.

In the first setup, the robot using the baseline model failed to reach the end and got stuck when first enters the patch area, while our model is able to succeed. A closer look in the right figure reveals that our model reduces $K_{stanley}$ when the robot enters the low frictional area and detects slip. It makes sense as when slip happens, heavy steering will not help much and could worsen the slip. A good tuning on $K_{stanley}$ and K_{speed} helps the robot to control the slip and succeed in the tracking task in this case. And it is up to the RL module to decide when and how much to tune the two gains. Also, the RL module does not have prior knowledge of the location of low-frictional area, and it is able to tune the gains based on current tracking status and reduce lateral error successfully.

Similar observation can be made in the second setup. Both models succeeded in the task, but the baseline model induced more lateral error when the robot entered low-frictional area, because it did not lower $K_{stanley}$ accordingly.

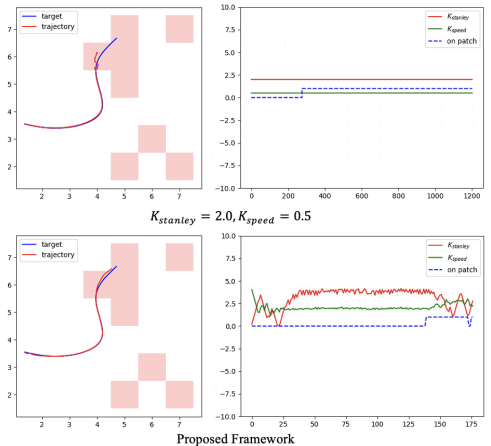


Fig. 8. Trajectory Comparison 1. The left figures show the bird-view map. The red patches correspond to the low frictional area. The right figures show how the gains evolve versus time. The blue dotted line indicates when the robot is on the low frictional patch. A value of 1 indicates the robot is on patch.

4. DISCUSSION

The experiments conducted show that simultaneous and online tuning of gains are necessary for mobile robot trajectory tracking under slippery conditions. Our model is able to tune the gains in lateral and longitudinal controls, and beat the baseline model in terms of lateral error metrics.

To reason the need of simultaneous gain tuning, consider when the robot is slipping or trajectory contains a large curvature. Both acceleration and steering commands should be considered to achieve an optimal tracking performance. For instance, with a large curvature, speed regulation can be relaxed while the steering command

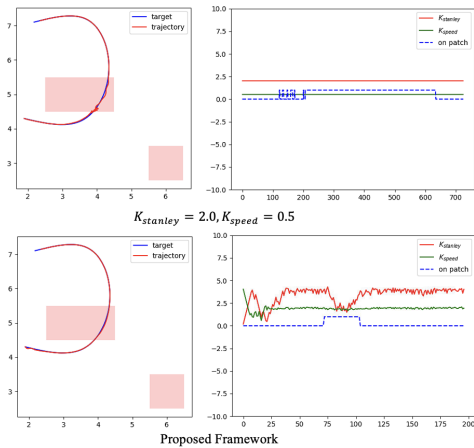


Fig. 9. **Trajectory Comparison 2.** Using online tuning instead of fixing gains alleviates deviation when the robot enters the slippery area. \bar{e} for baseline and proposed framework are 0.0247 and 0.0112, respectively. e_{max} are 0.0624 and 0.0336, respectively.

needs to have a bigger gain. Or when robot is slipping, both gains might need to be adjusted, as seen in Fig. 8 and 9. The magnitude of commands needs to be determined simultaneously, and the RL module in our framework decides the magnitudes of both gains at each timestep.

Also notice for some metrics such as $\overline{\Delta u}$ and $\overline{\Delta u}_{slip}$, K_{speed} tuning dominates the performance. One reason is that speed regulation impacts the wheel velocity change more than angular regulation, because sometimes the curvature is not very abrupt for steering to change much, but speed has to be regulated all the time.

We showed our framework is able to improve \bar{e} , e_{max} , \bar{e}_{slip} by 6.6%, 12.7%, and 4.7%, respectively. However the command and speed stability during slipping were compromised a bit. It makes sense as the robot tries to relax other constraints in order to reduce the lateral error. In many mobile robot slipping scenarios such as in a factory setting, the most important aspect is to reduce the lateral error because deviations could lead to robot hitting unwanted objects and causing harms. Therefore a lower stability in speed and command are acceptable.

5. CONCLUSION AND FUTURE WORK

To reduce slip for mobile robots, we propose a hierarchical framework that utilizes an RL module to adapt gains for the tracking controllers simultaneously online. We demonstrated the necessity of simultaneous gain tuning, and showed that our online framework outperforms the best baseline model using fixed gains, especially in terms of long and short term lateral errors.

REFERENCES

Abdelmoniem, A., Osama, A., Abdelaziz, M., and Maged, S.A. (2020). A path-tracking algorithm using predictive stanley lateral controller. *International Journal of Advanced Robotic Systems*, 17(6), 1729881420974852.

Cai, P., Mei, X., Tai, L., Sun, Y., and Liu, M. (2020). High-speed autonomous drifting with deep reinforcement learning. *IEEE Robotics and Automation Letters*, 5(2), 1247–1254.

Carlucho, I., De Paula, M., and Acosta, G.G. (2019). Double q-pid algorithm for mobile robot control. *Expert Systems with Applications*, 137, 292–307.

Chang, H., Xu, Z., and Tomizuka, M. (2020). Cascade attribute network: Decomposing reinforcement learning control policies using hierarchical neural networks. *IFAC-PapersOnLine*, 53(2), 8181–8186.

Coumans, E. and Bai, Y. (2016–2021). Pybullet, a python module for physics simulation for games, robotics and machine learning. <http://pybullet.org>.

Gao, H., Zhou, R., Tomizuka, M., and Xu, Z. (2022). Reinforcement learning based online parameter adaptation for model predictive tracking control under slippery condition. In *2022 American Control Conference (ACC)*, 2675–2682. IEEE.

Kim, J. and Lee, J. (2016). A kinematic-based rough terrain control for traction and energy saving of an exploration rover. In *2016 IEEE/RSJ International Conference on Intelligent Robots and Systems (IROS)*, 3595–3600. IEEE.

Nandy, S., Shome, S., Somani, R., Tanmay, T., Chakraborty, G., and Kumar, C. (2011). Detailed slip dynamics for nonholonomic mobile robotic system. In *2011 IEEE International conference on mechatronics and automation*, 519–524. IEEE.

Pico, N., Jung, H.r., Medrano, J., Abayebas, M., Kim, D.Y., Hwang, J.H., and Moon, H. (2022). Climbing control of autonomous mobile robot with estimation of wheel slip and wheel-ground contact angle. *Journal of Mechanical Science and Technology*, 36(2), 959–968.

Sakai, A., Ingram, D., Dinius, J., Chawla, K., Raffin, A., and Paques, A. (2018). Pythonrobotics: a python code collection of robotics algorithms. *arXiv preprint arXiv:1808.10703*.

Sebastian, B. and Ben-Tzvi, P. (2019). Active disturbance rejection control for handling slip in tracked vehicle locomotion. *Journal of Mechanisms and Robotics*, 11(2), 021003.

Tang, C., Xu, Z., and Tomizuka, M. (2019). Disturbance-observer-based tracking controller for neural network driving policy transfer. *IEEE Transactions on Intelligent Transportation Systems*, 21(9), 3961–3972.

Tian, Y., Sidek, N., and Sarkar, N. (2009). Modeling and control of a nonholonomic wheeled mobile robot with wheel slip dynamics. In *2009 IEEE Symposium on Computational Intelligence in Control and Automation*, 7–14. IEEE.

Wang, S. and Zhai, J. (2020). A trajectory tracking method for wheeled mobile robots based on disturbance observer. *International Journal of Control, Automation and Systems*, 18(8), 2165–2169.

Xu, Z., Tang, C., and Tomizuka, M. (2018). Zero-shot deep reinforcement learning driving policy transfer for autonomous vehicles based on robust control. In *2018 21st International Conference on Intelligent Transportation Systems (ITSC)*, 2865–2871. IEEE.

Xu, Z., Yu, W., Herzog, A., Lu, W., Fu, C., Tomizuka, M., Bai, Y., Liu, C.K., and Ho, D. (2021). Cocoli: contact-aware online context inference for generalizable non-planar pushing. In *2021 IEEE/RSJ International Conference on Intelligent Robots and Systems (IROS)*, 176–182. IEEE.